Validation of Afterbody Aeroheating Predictions for Planetary Probes: Status and Future Work

Michael J. Wright,[(1)] James L. Brown,[(1)] Krishnendu Sinha,[(3)] Graham V. Candler,[(3)] Frank S. Milos,[(1)] Dinesh K. Prabhu[(2)]

[(1)] *NASA Ames Research Center, MS 230-2, Moffett Field, CA 95050*
[(2)] *ELORET Corp., 970 W. Fremont, Suite 8, Sunnyvale, CA 94087*
[(3)] *University of Minnesota, 107 Akerman Hall, Minneapolis, MN 55455*

ABSTRACT

A review of the relevant flight conditions and physical models for planetary probe afterbody aeroheating calculations is given. Readily available sources of afterbody flight data and published attempts to computationally simulate those flights are summarized. A current status of the application of turbulence models to afterbody flows is presented. Finally, recommendations for additional analysis and testing that would reduce our uncertainties in our ability to accurately predict base heating levels are given.

1. INTRODUCTION

Uncertainty levels associated with aeroheating predictions for the design of the afterbody of planetary probes are typically assumed to be in the range of 200-300%, a level that can have a significant impact on Thermal Protection System (TPS) material selection and weight. This conservatism in the afterbody heat shield design will also shift the center of gravity afterward, which reduces the stability of the probe and in some circumstances may necessitate the addition of ballast in the nose. Current design practice for an afterbody heatshield assumes a laminar, fully catalytic, non-ablating surface. The predictions thus obtained are then augmented by a large factor of safety to account for turbulent transition, material response, and uncertainties in the baseline computations. A primary reason for this uncertainty is a sparsity of data for validation of our computational tools. Ground test data are usually complicated by sting interference effects. Little flight data exist, and recent attempts to propose dedicated flight experiments have failed to reach fruition. Therefore, it is important to thoroughly understand the limited flight data that are available to improve the design fidelity of the next generation of Earth and planetary entry vehicles and to assess the need for additional focused flight testing.

This paper will discuss four general topics. First, we review the relevant flow regimes and physical models for afterbody flows. Next, the paper surveys the available flight data for validating afterbody-heating predictions and reviews prior computational analyses of these data. Then, we conduct a brief survey of the state of the art in computing turbulent afterbody flowfields. Finally, we provide recommendations for areas of further work, and possible flight data that would aid in reducing the afterbody aeroheating design uncertainty.

2. FLOW REGIMES AND PHYSICAL MODELS

During entry, a planetary probe will pass from a free-molecular (collisionless) to a non-continuum and finally to a continuum flow regime. The transition between these regimes is usually determined by evaluation of the freestream Knudsen number $Kn_\infty = \lambda_\infty / D$, where λ_∞ is the mean free path and D is the body diameter. Free molecular flow is usually defined as the region where $Kn_\infty > 100$, while continuum flow is usually defined as the region where $Kn_\infty < 0.01$. This criterion is not accurate for separated base flows, because the local mean free path in the separation region can be much larger than that in the freestream. A more accurate determination can be made by using the density (ρ) gradient length local Knudsen number[1]

$$Kn_{GLL} = \frac{\lambda}{\rho} \left| \frac{d\rho}{dl} \right|_{max} \qquad (1)$$

where λ and ρ are local values and the derivative is evaluated along the maximum gradient direction. Following the work of Boyd et al.,[1] we assume that continuum breakdown occurs when $Kn_{GLL} > 0.1$. This criterion results in a more useful determination of continuum breakdown in a separated flow, because while the local mean free path in the separation region can be quite large, the density gradient is usually small, which delays the onset of non-continuum effects. For afterbody flows the highest values of Kn_{GLL} are typically observed near the flow separation point due to large density gradients. Numerical solutions for free molecular and non-continuum flows are typically obtained using a Direct Simulation Monte Carlo (DSMC) methodology. An excellent review on the status of DSMC calculations for non-continuum wake flows was presented by Moss and Price.[2] However, for

many problems of interest the majority of the aeroheating occurs in continuum flow, where Navier-Stokes based computational fluid dynamics (CFD) methods are applicable. The remainder of this paper will deal with the continuum flow regime.

When a probe enters a planetary atmosphere at high velocity, the resulting shock wave will thermally excite, dissociate, and possibly ionize the gas. In order to accurately model the resulting flowfield including the wake of the probe a non-equilibrium model is usually required.[3] Each chemical and thermal relaxation process has an associated characteristic time, and the rapid expansion of the flow into the wake will decrease the collision rate, which freezes the slower processes (such as vibrational relaxation) while the faster chemical relaxation processes continue at a finite rate. The details of the base flow structure and resulting heating rates can be very sensitive to the non-equilibrium state of the gas.[4] An excellent review of the thermodynamic and chemical-kinetic models for a non-equilibrium flowfield is given by Gnoffo et al.[5]

The afterbody flowfield will likely transition from a laminar to a turbulent flow during the entry. Wake transition begins in the far wake and travels upstream with increasing freestream Reynolds number (*Re*) until reaching the neck, where it is (temporarily) stopped by the adverse pressure gradient. In the base region transition begins in the separation shear layer. Lees[6] gives a transition correlation for the free shear layer in a two-dimensional or axisymmetric flow that is based on a local transition Reynolds number, defined as

$$\mathrm{Re}_{tr} = \rho_e u_e L / \mu_e \tag{2}$$

where *L* is the running length of the shear layer from the separation point and the local density, velocity and viscosity are evaluated based on fluid properties at the outer edge of the shear layer. The critical transition Reynolds number is a function of the edge Mach number, and ranges from about 2×10^4 at Mach 2 to 5×10^6 at Mach 5. This criterion is based on free-flight data, but does not include effects of upstream ablation product gas injection, which could have a destabilizing effect on the shear layer and separated flow region.

Low *Re* wake flows are steady and dominated by a small number of large vortices. As the freestream Reynolds number increases the extent of separation increases as well and the vortex structure becomes more complex. Eventually the vortices begin to oscillate and the base flow becomes unsteady. Typically, the Reynolds number at which the flowfield becomes
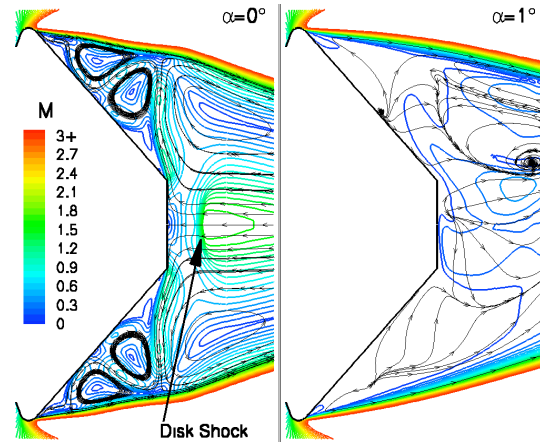

Fig. 1. Computed Mach number contours and streamlines in the symmetry plane of the Mars Pathfinder entry probe.

unsteady is near that at which transition to turbulence is predicted to begin. For many cases of interest, both events occur after the peak heating point on the trajectory. For these cases much of the heat pulse can be simulated assuming a continuum, laminar, steady flow.

Computational simulations of axisymmetric base flows with a flat base frequently show a disk shock in the near wake, caused when the reverse flow becomes supersonic along the rear stagnation line and a normal shock is required to slow the gas before impacting the body. The computed pressure and heat transfer on the flat base for these cases are much higher than would be the case if the disk shock were not present. Free flight experiments do not appear to show evidence of such a disk shock, although it would be difficult to see such a weak shock in a conventional Schlieren image. Clearly, since the presence of a disk shock has a significant influence on the predicted base heating, it is important to understand whether such a phenomenon is real or merely a computational artifact. One possibility is that the disk shock is a neutrally stable solution of the Navier-Stokes equations, which can occur only for an identically axisymmetric flowfield. Since no real flow is ever completely axisymmetric, this solution would rarely (if ever) occur in nature. In order to test this theory, two simulations were performed for Mars Pathfinder (Fig. 1). Freestream velocity is 6.6 km/s and density is 2.8×10^{-4} kg/m^3. The first solution was run assuming axisymmetric flow, and clearly shows the disk shock in the wake. The second was run as a three-dimensional flow at $\alpha = 1°$, and no disk shock is present for this case. In addition, the computed pressure and heat transfer on the flat base are a factor of three lower for the $\alpha = 1°$ solution. This result lends some support to the present hypothesis; however, the problem of disk

shocks in axisymmetric base flows requires further study, including systematic comparison with experimental base heating and pressure data.

Finally, wake flows are sensitive to the details of the volume grid used in the CFD analysis. Therefore it is important to generate a grid that is well aligned to anticipated flow features. In particular, it is extremely important that the grid have sufficient points in the shoulder region to capture the rapid expansion and accurately predict the flow separation point and the angle of the resulting shear layer.[7] There must also be sufficient points in the separated flow region to resolve the vortical structure and the wake compression, or neck. At higher Reynolds numbers the wake will consist of multiple counter-rotating vortices that must be resolved. Care must also be taken to ensure that the grid completely encloses the subsonic portion of the wake, which can extend several body diameters downstream.

3. AVAILABLE FLIGHT DATA & PREVIOUS VALIDATION ATTEMPTS

Most relevant flight data for validation of afterbody aeroheating predictions was obtained during the Apollo program, although there are also limited data from other European and American entry probes. It is likely that Russian flight data also exist, although no references to any such data were located in the open literature. This section summarizes the available flight data, and discusses published attempts at post-flight analysis.

Table 1 Launch dates and entry conditions for Apollo program flight tests.

Flight	Launch Date	V (km/s)	α (deg)	γ (deg)	Refs
Fire-I	Apr. 14, 1964	11.56	0	-14.7	1,2,5
Fire-II	May 22, 1965	11.35	0	-14.7	3,4,14
AS-201	Feb. 26, 1966	7.67	20	-8.6	22
AS-202	Aug. 25, 1966	8.29	18	-3.5	22,25,27
Apollo 4	Nov. 9, 1967	10.73	25	-5.9	23,26,29
Apollo 6	Apr. 4, 1968	9.60	25	-6.9	23

3.1 Project Fire

Project Fire was an Apollo technology demonstrator program that resulted in two ballistic entry test flights, Fire-I[8-9] and Fire-II.[10-11] The primary objective of Project Fire was to understand the radiative heating environment of an Earth entry vehicle at Lunar return velocities, but the silica-phenolic afterbody was also instrumented with nine surface mounted thermocouples, one pressure sensor, and a radiometer. Table 1 shows the launch dates and entry conditions for the two Project Fire flight tests, and Figure 2 shows the vehicle
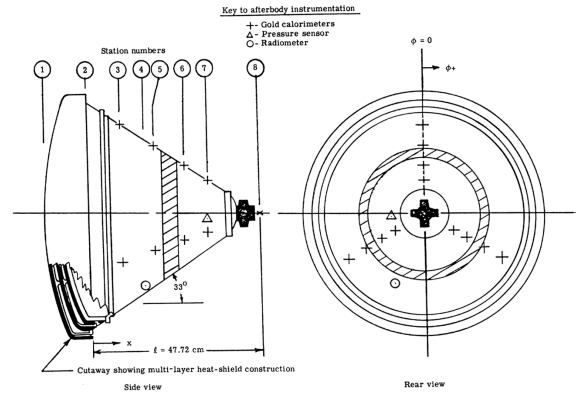

Fig. 2.   Schematic of Fire reentry vehicle showing instrument placement (from [11]).
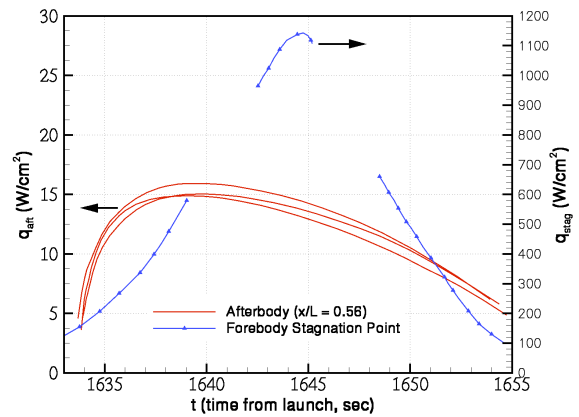

Fig. 3. Time histories of heat transfer measured during Fire-II flight on the conical frustum and at the forebody stagnation point (from [13]).

geometry and afterbody instrument placement. Unfortunately, the Fire-I probe experienced large angle of attack variations during entry, apparently due to a stage-separation anomaly in which the booster entered in front of the capsule, making the data from this flight difficult to interpret.[12] In contrast, the Fire-II entry was extremely successful. The vehicle maintained an angle of attack of less than 1° through the majority of the high heating portion of the entry, increasing to about 11° by the end of the experiment.[11] All afterbody instrumentation was functional during this flight, providing a valuable database of afterbody heating for a ballistic entry vehicle. Figure 3 shows the time histories of total heat transfer measured during flight at one afterbody station, and also at the forebody stagnation point. Peak afterbody heating at this location was about 1.5% of the peak stagnation point heating. The afterbody radiometer was determined to be functional, but did not measure any signal during the heating portion of the entry, indicating that radiative heating to the afterbody was negligible at these conditions.[11]

277
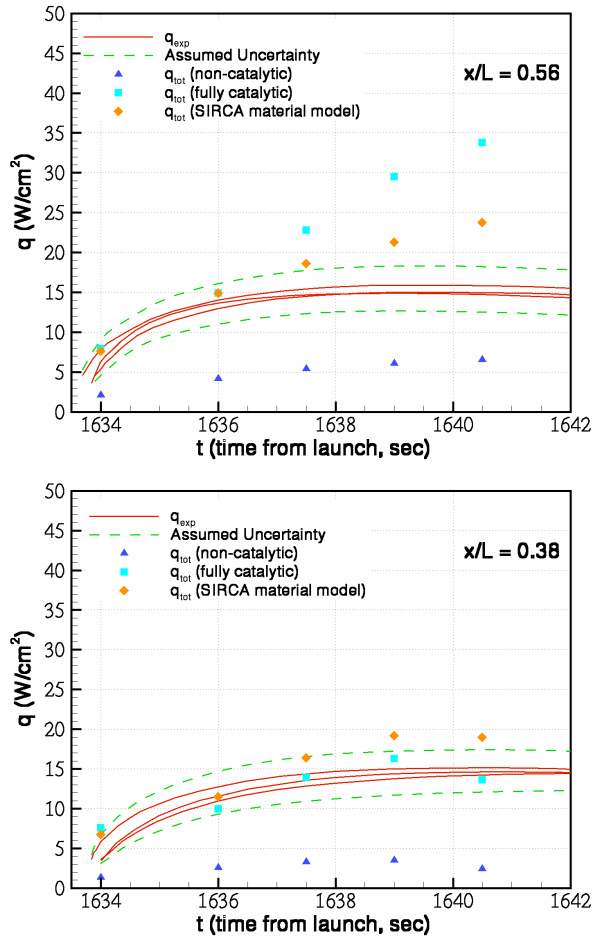
Fig. 4. Time histories of total heat transfer for Fire-II computed using several catalysis models on the afterbody as compared to flight data at two axial locations (from [13]).

The Fire-II afterbody flight data were analyzed in detail by Wright et al.[13] using a nonequilibrium Navier-Stokes code. The CFD results were computed assuming laminar flow, an assumption validated using the correlation of Lees.[6] A partially catalytic afterbody surface was assumed, with the catalytic efficiency of the afterbody TPS approximated using analogies to similar currently manufactured materials. Figure 4 shows the results of this analysis for two afterbody locations. The computations agreed with the flight data to within the experimental uncertainty over the early portion of the trajectory ($t < 1638$ s). The computations overpredicted the flight data later in the trajectory, especially on the rear of the body (larger x/L), but this result was attributed to TPS ablation, which was not modeled in the simulations.[13] The results demonstrated that modern CFD methods are capable of reproducing the flight data to within experimental accuracy as long as realistic surface boundary conditions are employed. A
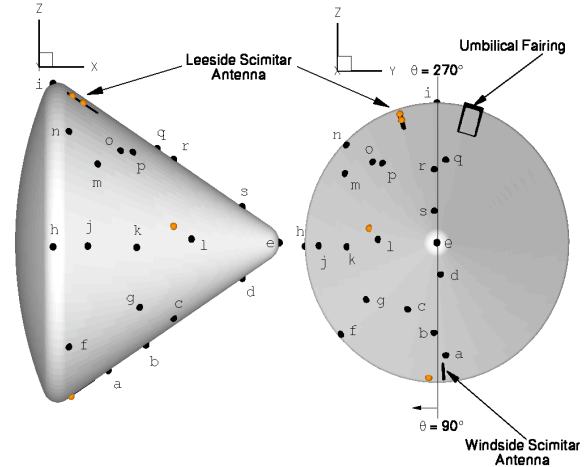

Fig. 5. Calorimeter locations on AS-201/202 afterbody. Orange symbols indicate inoperative instruments during AS-202 (from [19]).

more recent preliminary computation of the turbulent portion of the trajectory has also been published;[14] the results will be discussed in the following section.

3.2 Apollo Program

The Apollo program sponsored several dedicated flight tests to understand the heating environment of orbital and super-orbital entry probes. Once the design of the Apollo Command Module was determined, four flight tests were conducted which included forebody and afterbody instrumentation. The first two, AS-201 and AS-202, were conducted at orbital velocities, while the final two, Apollo 4 and Apollo 6, were conducted at super-orbital velocities representative of Lunar return. Table 1 shows the relevant entry parameters for these tests. The four flights together constitute the best database of flight afterbody heating data obtained to date. An onboard Inertial Measurement Unit (IMU) during the last three flights enabled an accurate trajectory reconstruction, and sounding rockets were used to reconstruct atmospheric properties.[15-16] The range of entry velocities and flight path angles during these flights were sufficient to span multiple flow regimes, from laminar to fully turbulent, and from minimal material response to strong pyrolysis injection and char formation. This range of conditions will permit a systematic study of the effects of turbulent transition and pyrolysis gas injection on turbulent heating levels.

The afterbody instrument package for AS-201 and AS-202 consisted of 23 surface-mounted calorimeters and 24 pressure transducers.[17] Calorimeter locations are shown in Fig. 5. Both flights were highly successful, with 16 of the calorimeters returning useful data on AS-201 and 19 on AS-202.[17] Pressure data were also

obtained during the AS-201 flight, but the dynamic pressure during the AS-202 mission was too low for meaningful readings to be obtained on the afterbody. The afterbody heating rates for AS-201 were much higher than those for AS-202 due to the steeper entry angle, and therefore the heating for this mission was significantly affected by charring of the TPS.[18]

The afterbody heating data for AS-201 have not been investigated in detail using modern CFD methods. However, a recent paper analyzed the data for AS-202.[19] A total of 15 three-dimensional CFD solutions were run spanning the time from the onset of continuum flow until the separation region became unsteady. The surface was assumed to be fully catalytic, which was a reasonable assumption for the hydrocarbon-resin based Avcoat TPS material. The results were computed assuming laminar flow, validated using the correlation of Lees.[6] The computations generally agreed with the flight data to within the experimental uncertainty (±20%) for 15 of the 19 functional calorimeters.[19] The results at three calorimeter locations are shown in Fig. 6. The first (calorimeter "a") was in an attached flow region, the second ("m") was in separated flow, and the third ("j") was at a location where the flow separated and reattached during the entry. The heat pulse has two distinct lobes due to an atmospheric skip maneuver performed by the spacecraft during entry. Interestingly, both the flight data and the CFD results at calorimeter "j" clearly show the reattachment at t = 4600 s and separation at t = 4800 s, which indicates that the CFD solutions are not only accurately predicting the magnitude of the heating, but also the extent of separation. Relatively poor agreement was obtained for two calorimeters near the rear apex of the vehicle; the reason is not known at this time but it may be due to unmodeled details of the apex geometry. This work again demonstrated the ability of modern computational methods to accurately predict afterbody heating levels.

The Apollo 4 and 6 test flights were intended to qualify the entry system for Lunar return by entering at α=25° and a relative velocity of about 11 km/s. The actual entry velocity for Apollo 6 was only about 9.6 km/s due to a re-ignition failure in the upper stage.[20] The instrument package was modified for these flights, and consisted of 21 calorimeters, 10 pressure transducers, and 2 radiometers. The locations of the instrumentation are shown in Fig. 7. All 21 calorimeters provided useful data on each flight. Four of the calorimeters were placed near simulated protuberances and gaps in the flight vehicle; these data may be useful to validate the ability of modern CFD to predict local heating around geometrical singularities. The remaining calorimeters
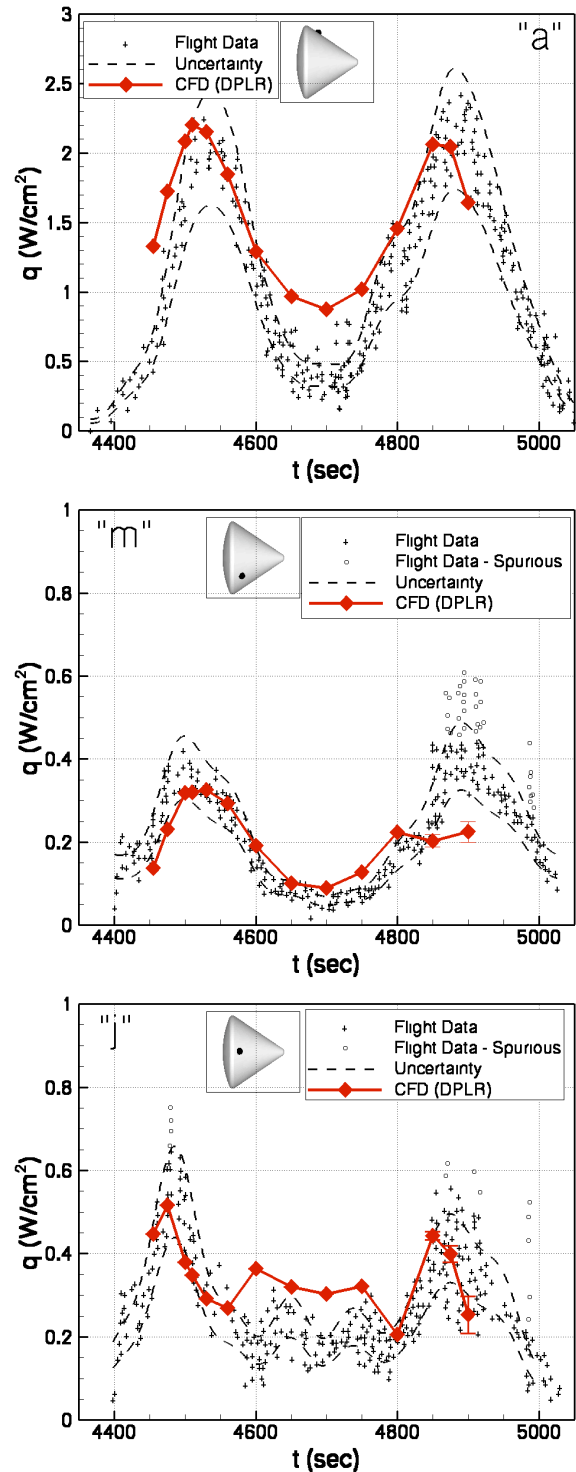

Fig. 6. Comparison of flight data and computed heat transfer for AS-202. Letters indicate calorimeter ID in Fig. 4 (from [19]).
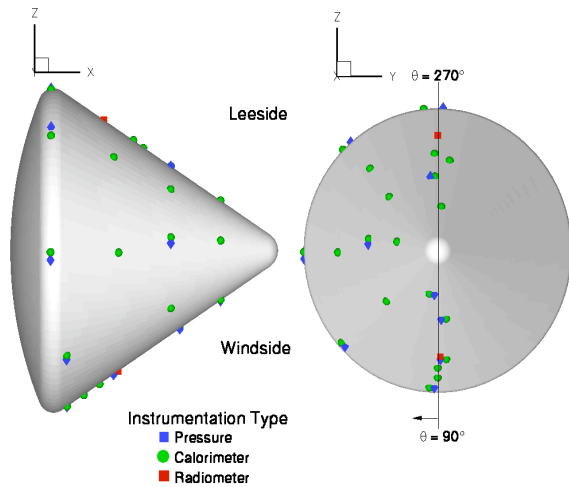
Fig. 7. Instrumentation locations on Apollo 4 and Apollo 6 conical afterbody.
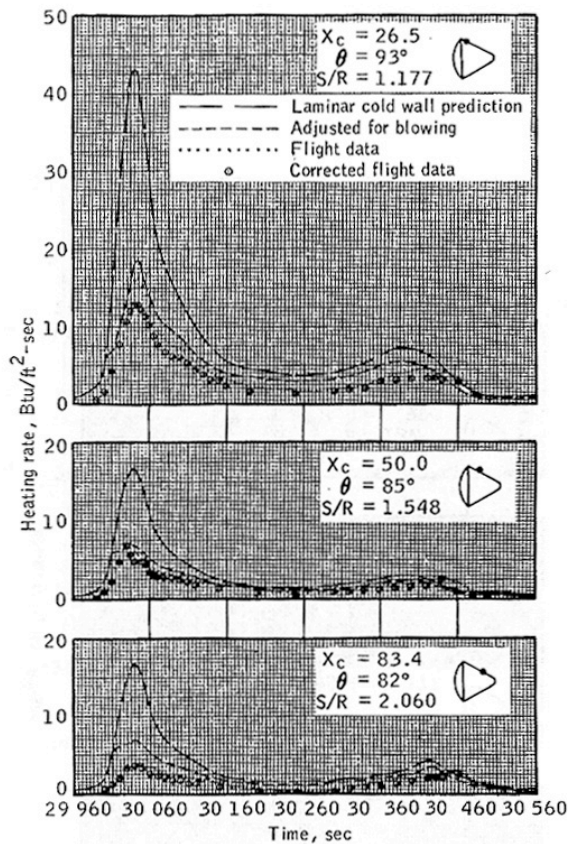

Fig. 8. Flight data and pre-flight engineering predictions from the Apollo 4 entry at three calorimeter locations on the attached flow portion of the afterbody (from [20]).

provided flight data of afterbody heat transfer on an ablating TPS material. The afterbody radiometers for both flights failed to detect a measurable signal,
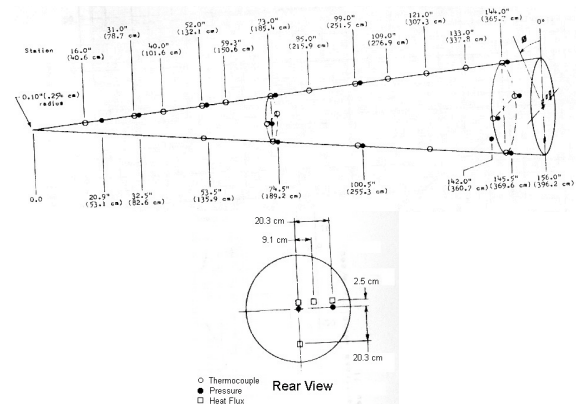

Fig. 9. Instrument locations on the Reentry F flight experiment (from [23]).

although they were determined to be functional. This result confirmed pre-flight predictions of negligible radiative heating,[21] and implies that there was zero afterbody radiative heating on the lower velocity AS-201 and AS-202 flights as well. There was little charring on the separated flow portion of the afterbody, and total heating levels were between 1-2% of stagnation point theory. The pressure and total heat transfer measured on the charred (attached flow) regions of the afterbody were corrected for wall blowing, but the resulting data were significantly lower than the preflight computations (see Fig 8). The level of underprediction was determined to be proportional to the forebody heating rate. Although a definitive reason for this effect has not been identified, it has been postulated that the cause was upstream blowing of ablation products into the boundary layer.[20,22] The afterbody heating data from these flights have yet to be looked at in detail with modern computational methods.

3.3 Other U.S. Flights with Afterbody Data

The Reentry F flight test was launched on April 27, 1968 from Wallops Island and entered at a relative velocity of 6 km/s on a ballistic trajectory.[23] The entry vehicle was a 3.92 m long 5° half-angle beryllium cone with a graphite nose tip, designed to provide transition and turbulent heat transfer data. The cone was instrumented with thermocouples and pressure sensors at 21 measurement stations, while the base had a total of 4 heat flux and 2 pressure sensors.[23] Instrument locations are shown in Fig. 9. Post-flight analysis of these data were somewhat complicated by thermal distortions, which resulted in a small effective angle of attack.[24] To date no comprehensive analysis of the base heating and pressure data given in [25] has been attempted with modern CFD tools.

The Viking program included two landers that entered the Martian atmosphere in July and September of 1976.
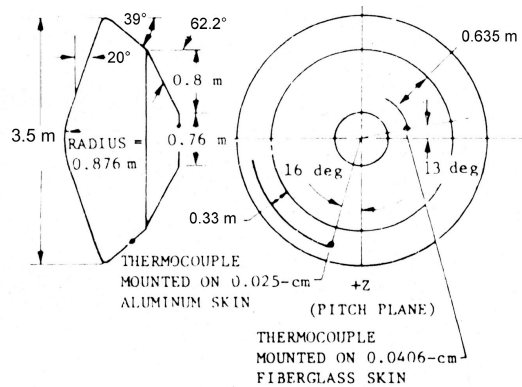
Fig. 10. Schematic of Viking entry probe showing sensor locations. (from [28]).
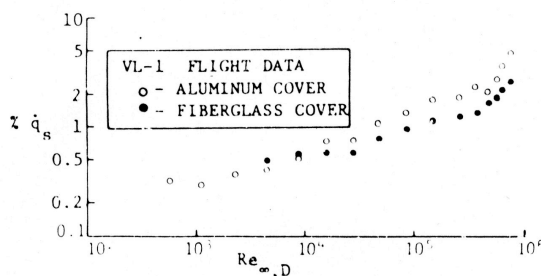
Fig. 11. Flight data from the afterbody temperature sensors on Viking 1. (from [27]).

Both probes were 70° sphere-cones which flew a lifting entry at a nominal angle of attack of 11°, and entered at a relative velocity of about 4.5 km/s.[26] Each probe included a base pressure sensor and two surface-mounted temperature sensors – one on the fiberglass inner cone and one on the aluminum skin of the outer cone.[27] A schematic of the Viking entry probe showing the temperature sensor locations is given in Fig. 10. Pre-flight analysis predicted afterbody heating to be 3% of the forebody stagnation point heating rate, but flight data indicated that the peak heating was actually about 4.2% of the stagnation value, as shown in Fig 11. The high heating levels, as well as the slope change observed in heating rate vs Reynolds number at $Re_D \sim 5 \times 10^5$, were believed to be evidence of turbulent transition on the base.[28] No attempt to reproduce these data with modern CFD techniques has been published.

The Galileo mission was launched October 18, 1989. The on-board 45° sphere-cone probe successfully entered the Jovian atmosphere on December 7, 1995 on a ballistic trajectory at a relative velocity of 47.4 km/s.[29] This probe survived the most severe heating environment ever experienced by a planetary entry capsule, with a peak ablating heat flux on the order of 30 kW/cm². Instrumentation consisted of 10 analog resistance ablation (ARAD) sensors on the forebody
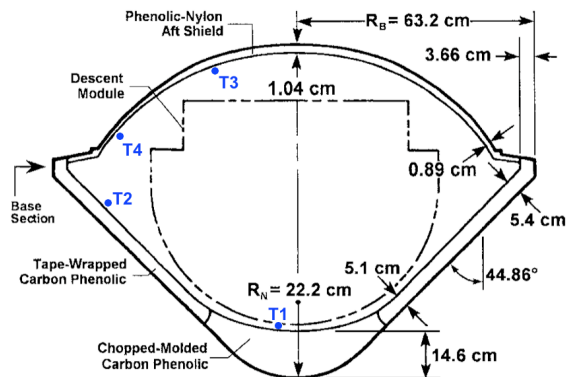
Fig. 12. Schematic of Galileo probe with thermometer locations marked (adapted from [30]).

and 4 resistance thermometers bonded to the structure beneath the carbon-phenolic TPS, as shown in Fig. 12. Both afterbody thermometers (T3 and T4 in Fig. 12) appeared to function normally. The only post-flight analysis of this data to date was performed by Milos et al.,[30] in which the thermometer response was simulated using a transient material response code coupled to a finite-element thermal analysis package. CFD analysis of the external flowfield was not performed. Instead, a triangular heat pulse was assumed with a total heat load based on engineering predictions. The results in [30] indicate that the post-flight analysis was not in good agreement with the afterbody flight data. Although it was possible to bound the flight data by varying the heat load and initial cold-soak structural temperature, Milos et al. were unable to reproduce the slope of the temperature increase. It remains to be seen whether a high-fidelity aerothermal analysis could improve the agreement with the flight data, although it should be noted that the Galileo flowfield is an extremely complex mix of optically thick radiation, strong ablation, and turbulent flow, and will present a significant challenge to the state of the art CFD methodology.

Mars Pathfinder was launched December 4, 1996 and successfully entered the Martian atmosphere on July 4, 1997 on a ballistic trajectory at a relative velocity of 7.5 km/s.[31] There was no surface-mounted instrumentation, but the aeroshell did contain nine thermocouples (TC) and three platinum resistance thermometers (PRT) at various depths in the TPS material as shown in Fig. 13. Of those on the afterbody, usable data were obtained from TC9, PRT1, and PRT3. Time histories of the temperature data at these locations are given in [32]. The only post-flight analysis of this data to date was performed by Milos et al.[32] In this analysis afterbody heating estimates were scaled from forebody CFD solutions. Using this assumption, Milos et al.[32] were able to reproduce the peak temperature at TC9, but not
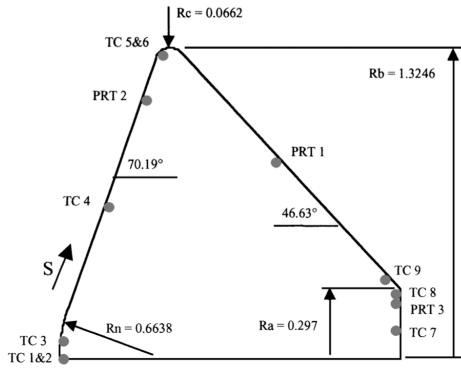
Fig. 13. Mars Pathfinder schematic showing instrument locations (from [32]).

the time history of the temperature response. However, by assuming a "best-fit" heating profile that was longer in duration than the scaled profile they were able to demonstrate excellent agreement with the flight data. The assumed shape of the "best-fit" profile was in general agreement with pre-flight predictions,[33-34] but the heating rates required to match the data were considerably lower. To our knowledge no attempt has been made to reconcile this discrepancy.

3.2 European Flight Data

The MIRKA capsule was a German-led low-cost flight test flown as a piggyback payload on a Russian FOTON capsule. MIRKA successfully reentered the Earth's atmosphere on a ballistic trajectory at a velocity of 7.6 km/s on October 23, 1997.[35] The capsule, shown schematically in Fig. 14, was essentially a one meter diameter sphere with a flat base. The capsule was instrumented with 2 pyrometers, 3 rarified flow experiment (RAFLEX) pressure probes, and 25 thermocouples (TC) integrated into the TPS material at varying depths.[35] A total of seven TC's were on the afterbody. Several simulations of the MIRKA flight data have been published,[36-38] although most researchers have dealt only with the forebody flow. It was noted in [36] that the heat flux readings at TC15-17 were strongly influenced by hot pyrolysis gases injected upstream of that location, and it seems likely that those further downstream would also be affected.

The European Space Agency launched the Atmospheric Reentry Demonstrator (ARD) on October 12, 1998.[39] The probe reentered the Earth's atmosphere at a velocity of 7.5 km/s. ARD was a subscale Apollo-like capsule with a diameter of 2.8 m. The capsule afterbody was instrumented with 7 pressure sensors, 4 thermocouples, and 4 copper calorimeters.[40] In addition, the afterbody cone was coated with thermo-sensitive paint. Although the forebody thermocouples failed above
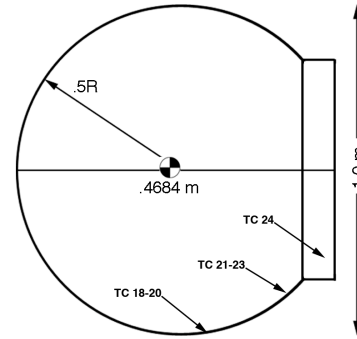

Fig. 14. Schematic of the MIRKA capsule with approximate location of aftbody thermocouples.

about 800° C, those on the afterbody were functional throughout the entry.[40] However, the deduced heat transfer is not considered to be reliable.[40] Better results were obtained from the calorimeters, which provided heat transfer data throughout the entry.[40] Computational analysis of the ARD afterbody has been presented in [40]. While good agreement was obtained between the computations and flight data early in the trajectory, the CFD overpredicted the peak flight heating by as much as a factor of two. Possible reasons given for this discrepancy were delayed transition to turbulence or an inadequate gas chemistry model.[40-41]

4. TURBULENT FLOW SIMULATIONS

All of the previous computational results discussed in this paper dealt exclusively with laminar afterbody flows. However, a significant increase in heating rate occurs with the transition from laminar to turbulent flow. For windward acreage heating of a hypersonic entry vehicle, this enhancement can be a factor of 3-4. Similar enhancement of base heating rates is also possible. Incorporation of proper modeling of both transition and turbulence into the computational analysis will, thus, have a considerable impact on the aeroshell design. Unfortunately, there have been few published attempts to simulate turbulent afterbody flight data with CFD methods. This section briefly discusses the application of both traditional and state of the art turbulence models to afterbody flowfields.

Brown[42] recently calculated a variety of experimental flows in order to assess various existing turbulence models for use with real-gas Navier-Stokes simulations of hypersonic reentry vehicles. The test cases were selected based on the relevance of flow geometry and conditions and based on an assessment of the confidence in experimental results. Turbulence models assessed included compressibility-corrected versions of the Baldwin-Lomax model,[43] the one-equation Spalart-

Allmaras model,[44] the Wilcox two-equation k-ω model,[45] and Menter's two-equation SST k-ω model.[46]

One of the selected cases was the Hollis and Perkins[47] afterbody experiment of Mach 9.8 flow over a 70° sphere-cone. The experimental configuration is similar to the Mars Pathfinder spacecraft, although it was sting mounted, which changes the dynamics of wake closure and provides a path for upstream influence via the subsonic boundary layer on the sting. The nominal conditions for this experiment are air at $M_\infty = 9.8$, $T_\infty = 52.45$ K, $\rho_\infty = 0.00868$ kg/m³, and a freestream Reynolds number of 9.2×10^4 based on diameter. The flow was assumed to be a perfect gas and an isothermal wall ($T_w = 300$ K) was specified.

Figure 15 shows Mach number contours from the SST turbulence model computation of the Hollis and Perkins experiment. The model surface is outlined in blue. Figure 16 shows the experimental heat transfer results along the model surface, along with the computed heat transfer for several of the turbulence models considered. The sting is included in the computations since the influence of the sting on the afterbody heat transfer results is likely to be significant. The flow is assumed to be laminar over the sphere-cone portion of the model. Separation occurs at the model shoulder ($s/R_b = 1$), and transition to turbulent flow is also specified to occur at this location. Reattachment occurs on the sting, with a recirculation zone washing most of the afterbody surface. The level of turbulence within the recirculation zone is obviously paramount to accuracy of the predictions for the afterbody heat transfer levels.

In Figure 16, the heat transfer results for the various turbulence models diverge considerably in the afterbody and sting reattachment regions. It is evident that the laminar and Baldwin-Lomax turbulent solutions under-predict heat transfer by as much as a factor of three in this region. The Spalart-Allmaras and k-ω models (not shown) similarly under-predicted the heat transfer in this region. Only the SST turbulence model accurately predicts the heat transfer over the entire afterbody and sting reattachment portions of this experiment, capturing the detailed variation on the afterbody frustum. Based on these results, as well as the other test cases chosen, Brown recommended the SST model for the computation of separated hypersonic flows.[42]

A particular shortcoming in afterbody turbulence model validation is the shortage of real-gas datasets. All of the datasets considered by Brown were amenable to treatment of the fluid as perfect-gas. Furthermore, although the Hollis and Perkins data are useful for
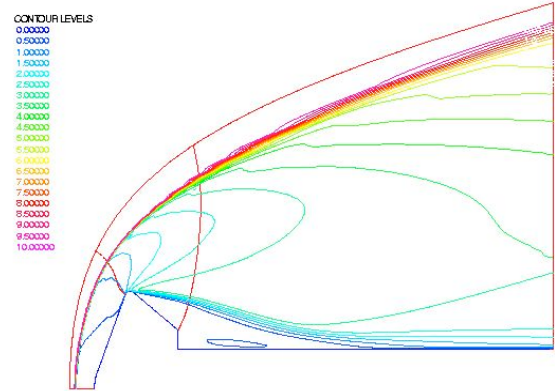
Fig. 15. Computed Mach Number contours for axisymmetric Mach 10, 70° Sphere-Cone of Hollis and Perkins (from [42]).
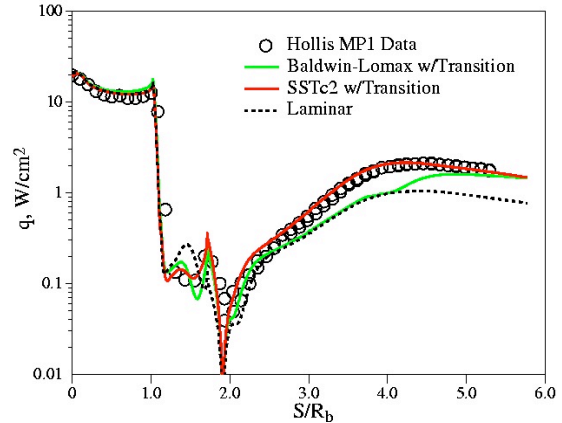

Fig. 16. Computed surface heat transfer for axisymmetric Mach 10, 70° Sphere-Cone of Hollis and Perkins (adapted from [42]).

afterbody heat transfer validation, the presence of the sting contaminates the assessment for heat transfer for the afterbody surfaces since closure of the recirculation zone is accomplished by attachment on the sting rather than with a free-flight wake closure.

Engineering prediction of turbulent flows relies heavily on Reynolds-averaged Navier-Stokes (RANS) simulations that compute the time-averaged flow field. However, RANS models can be inaccurate in high Reynolds number flows with large-scale separation. By comparison, detached eddy simulation (DES)[48] significantly improves predictions in massively separated flows by simulating the unsteady dynamics of the dominant length scales. DES methods have been shown to accurately predict the extent of the recirculation region and the base pressure in supersonic flows,[49] but such models have not been applied to hypersonic chemically reacting flowfields.
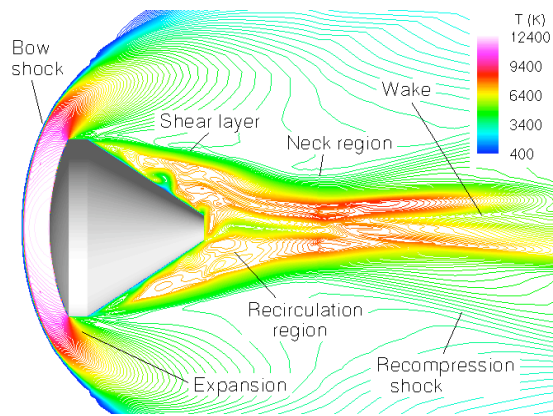
Fig. 17. Instantaneous pitch plane temperature contours around the Fire II vehicle computed with DES (from [14]).
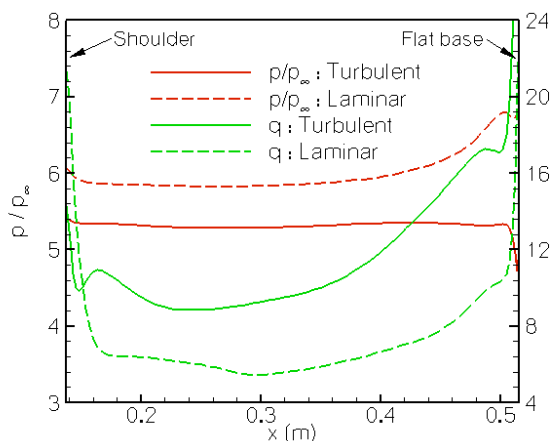

Fig. 18. Computed laminar and turbulent pressure and heat transfer on the afterbody of the Fire II vehicle (from [14]).

Recently Sinha et al.[14] used DES to study the flow field behind the Fire II flight vehicle at 35 km altitude, $M_\infty = 16$, and a freestream Reynolds number of 1.8×10^6 based on diameter. In these preliminary simulations the effect of non-equilibrium thermo-chemistry on the flowfield was neglected. The flowfield was simulated by solving the three-dimensional Favre-averaged Navier-Stokes equations. Turbulence was modeled using the Spalart-Allmaras one-equation turbulence model,[44] which was modified to operate in DES mode by introducing a new length scale d_{des}, defined as

$$d_{des} = \min(d, C_{des}\Delta) \tag{3}$$

where d is the distance to the nearest wall, Δ is the largest dimension of the local grid cell, and C_{des} is an adjustable parameter calibrated by Shur.[48] This new length scale results in a form of turbulent eddy viscosity close to that of a large eddy simulation far from solid boundaries, and smoothly reverts back to the original RANS model near the wall.

Figure 17 shows the instantaneous temperature contours in the pitch plane of the Fire II vehicle. The main flow features are identified in the figure. The flow separates at the beginning of the conical afterbody and a large recirculation region forms behind the vehicle. The flow in this region is highly unsteady and three-dimensional, and is characterized by vortices and shear layers of varying intensity and length scales. The temperature in the wake is relatively high (6000 - 9000 K) except for a thin region close to vehicle wall. This corresponds to a laminar boundary layer on the afterbody. Some of the cold fluid from this region is swept away from the wall.

Time-averaged flow data were also computed by integrating the unsteady flow field over multiple characteristic times. The resulting flowfield was not entirely symmetric about the vehicle axis, as would be expected for an axisymmetric vehicle at zero angle of attack. The reasons for this asymmetry are currently under investigation.[14] Figure 18 shows the computed time averaged base pressure and heat transfer for the turbulent and baseline laminar computations. The pressure on the afterbody is lower in the turbulent simulation than the laminar case, whereas the turbulent heat transfer rate is higher than the laminar by 60-70%. The present results are preliminary, but are a promising first step in the application of sophisticated turbulence models to hypersonic base flows.

5. CONCLUSIONS AND RECOMMENDATIONS

The data obtained during Project Fire and the Apollo program provide an invaluable resource for the validation of modern computational tools for afterbody aeroheating. The six flight tests provide data spanning the entire range of Earth entry conditions, from axisymmetric to three-dimensional, non-continuum to continuum, laminar to turbulent, and non-ablating to fully ablating. The European ARD and MIRKA flights, together with the American Reentry F, are an additional valuable resource for Earth entry base heating. Two recent papers have looked at a portion of the Fire and Apollo data and have shown that modern computational methods appear to be fully capable of predicting afterbody heating to within the uncertainty of the flight data, at least for laminar flows without ablation. There has been less work done on understanding turbulent wake flows. Recent efforts using conventional and advanced turbulence models summarized herein are a good first step; however, more work needs to be done to fully understand the flight data. Data from Reentry F, a

flat-based ballistic entry vehicle, may help to answer not only our ability to predict turbulent base heating, but also whether the disk shock phenomena is seen in flight. The Apollo 4 and 6 flight data include the effects of ablation and turbulence and will allow us to validate current methodologies in this environment. This work should be completed prior to recommending new flight testing so that we are better able to assess the gaps in our ability to predict Earth entry afterbody heating.

The state of affairs for other planetary destinations is not as good. Although code validation with Earth entry data certainly increases confidence in our ability to predict afterbody heating at other planets, differences in atmospheric composition and the associated chemical kinetics can only be fully resolved with in-situ flight data. Unfortunately, two thermo-couples on Viking and a single near-surface thermo-couple on Pathfinder are the only truly usable pieces of afterbody flight aeroheating data for any non-Earth entry. Worse, the recent trend has been a reduction or even elimination of heatshield instrumentation as a cost-saving or (perceived) risk-reduction measure. For example, there was no heat-shield instrumentation on either Mars Exploration Rover (MER) entry vehicle, the Stardust sample return capsule, or on the European Space Agency's Mars Beagle or Huygens Titan probes. Future planetary entry missions must include heatshield instrumentation in order to improve our understanding of these environments. The aftshell is often the safest place to incorporate instrumentation due to the low heating rates, and the results summarized in this paper give increased confidence in our ability to use such data effectively for code validation and improvement.

6. REFERENCES

[1] Boyd, I., Chen, G., and Candler, G., "Predicting Failure of the Continuum Fluid Equations in Transitional Hypersonic Flows," *Physics of Fluids*, Vol. 7, No. 1, 1995, pp. 210-219.

[2] Moss, J. and Price, J., "Review of Blunt Body Wake Flows at Hypersonic Low Density Conditions," AIAA Paper 96-1803, Jun. 1996.

[3] Gnoffo, P.A., "Planetary Entry Gas Dynamics," *Annual Review of Fluid Mechanics*, Vol. 31, 1999, pp. 459-494.

[4] Olynick, D., Chen, Y.-K., and Tauber, M., "Aerothermodynamics of the Stardust Sample Return Capsule," *Journal of Spacecraft and Rockets*, Vol. 36, No. 3, 1999, pp. 442-462.

[5] Gnoffo, P., Gupta, R., and Shinn, J., "Conservation Equations and Physical Models for Hypersonic Air Flows in Thermal and Chemical Nonequilibrium," NASA TP-2867, Feb. 1989.

[6] Lees, L., "Hypersonic Wakes and Trails," *AIAA Journal*, Vol. 2, No. 3, 1964, pp. 417-428.

[7] Gnoffo, P., Price, J., and Braun, R., "Computation of Near Wake Aerobrake Flowfields," *Journal of Spacecraft and Rockets*, Vol. 29, No. 2, 1992, pp. 182-189.

[8] Scallion, W.I. and Lewis, J.H., "Flight Parameters and Vehicle Performance for Project Fire Flight I," NASA TN D-2996, 1965.

[9] Slocumb, T.H., "Project Fire Flight I Heating and Pressure Measurements on the Reentry Vehicle Afterbody at a Velocity of 38,000 Feet Per Second," NASA TM X-1178, 1965.

[10] Lewis, J.H. and Scallion, W.I., "Flight Parameters and Vehicle Performance for Project Fire Flight II," NASA TN D-3569, 1966.

[11] Slocumb, T.H., "Project Fire Flight II Afterbody Temperatures and Pressures at 11.35 Kilometers Per Second," NASA TM X-1319, Dec. 1966.

[12] Woodbury, G., "Angle of Attack Analysis for Project Fire I Reentry Flight," NASA TN D-3366, 1966.

[13] Wright, M., Loomis, M., and Papadopoulos, P., "Aerothermal Analysis of the Project Fire II Afterbody Flow," *Journal of Thermophysics and Heat Transfer*, Vol. 17, No. 2, 2003, pp. 240-249.

[14] Sinha, K., Barnhardt, M., and Candler, G., "Detached Eddy Simulation of Hypersonic Base Flows with Application to Fire II Experiments," AIAA Paper 2004-2633, Jun. 2004.

[15] Hillje, E., "Entry Flight Aerodynamics from Apollo Mission AS-202," NASA TN D-4185, Oct. 1967.

[16] Hillje, E., "Entry Aerodynamics at Lunar Return Conditions Obtained from the Flight of Apollo 4," NASA TN D-5399, 1969.

[17] Lee, D., Bertin, J., and Goodrich, W., "Heat Transfer Rate and Pressure Measurements During Apollo Orbital Entries," NASA TN D-6028, Oct. 1970.

[18] Lee, D., "Apollo Experience Report: Aerothermodynamics Evaluation," NASA TN D-6843, Jun. 1972.

[19] Wright, M., Prabhu, D., and Martinez, E., "Analysis of Afterbody Heating Rates on Apollo Command Modules, Part 1: AS-202," AIAA Paper 2004-2456.

[20] Lee, D. and Goodrich, W., "Aerothermodynamic Environment of the Apollo Command Module During Superorbital Entry," NASA TN D-6792, Apr. 1972.

[21] Ried, R., Rochelle, W., and Milhoan, J., "Radiative Heating of the Apollo Command Module: Engineering Predictions and Flight Measurement," NASA TM X-58091, Apr. 1972.

[22] Lee, G., "Ablation Effects on the Apollo Afterbody Heat Transfer," *AIAA Journal*, Vol. 7, No. 8, 1969, pp. 1616-1618.

[23] Wright, R. and Zoby, E., "Flight Measurements of Boundary Layer Transition on a 5° Cone at a Mach Number of 20," NASA TM X-2253, May 1971.

[24] Alley, V. and Guillotte, R., "Postflight Analysis of Thermal Distortions of the Reentry F Spacecraft," NASA TM X-2250, May 1971.

[25] Dillon, J. and Carter, H., "Analysis of Base Pressure and Base Heating on a 5° Half Angle Cone in Free Flight Near Mach 20," NASA TM X-2468, Jan. 1972.

[26] Martin-Marietta Corp., "Viking Lander System, Primary Mission Performance Report," NASA CR-145148, Apr. 1977.

[27] Martin-Marietta Corp., "Entry Data Analysis for Viking 1 and 2," NASA CR-159388, Nov. 1976.

[28] Schmitt, D., "Base Heating on an Aerobraking Orbital Transfer Vehicle," AIAA Paper 83-0408.

[29] Givens, J., Nolte, L., and Pochettino, L., "Galileo Atmospheric Entry Probe System: Design, Development and Test," AIAA Paper 83-0098, Jan. 1983.

[30] Milos, F., Chen, Y.-K., Squire, T., and Brewer, R., "Analysis of Galileo Probe Heat Shield Ablation and Temperature Data," *Journal of Spacecraft and Rockets*, Vol. 36, No. 3, 1999, pp. 298-306.

[31] Spencer, D., Blanchard, R., Braun, R., Kallemeyn, P., and Thurman, S., "Mars Pathfinder Entry, Descent and Landing Reconstruction," *Journal of Spacecraft and Rockets*, Vol. 36, No. 3, 1999, pp. 357-366.

[32] Milos, F., Chen, Y.-K., Congdon, W., and Thornton, J., "Mars Pathfinder Entry Temperature Data, Aerothermal Heating, and Heatshield Material Response," *Journal of Spacecraft and Rockets*, Vol. 36, No. 3, 1999, pp. 380-391.

[33] Mitcheltree, R. and Gnoffo, P., "Wake Flow About Mars Pathfinder Entry Vehicle," *Journal of Spacecraft and Rockets*, Vol. 32, No. 5, 1995, pp. 771-776.

[34] Haas, B. and Venkatapathy, E., "Mars Pathfinder Computations Including Base Heating Predictions," AIAA Paper 95-2086, Jun. 1995.

[35] Schmitt, G., Pfeuffer, H., Kasper, R., Kleppe, F., Burkhardt, J., and Shottle, U., "The MIRKA Reentry Mission," IAF-98-V2.07, 49th International Astronautical Congress, Sep. 1998.

[36] Jahn, G., Schöttle, U., and Messerschmid, E., "Post-Flight Surface Heat Flux and Temperature Analysis of the MIRKA Reentry Capsule," *Proceedings of the 21st International Symposium on Space Technology*, Omiya, Japan, May 1998, pp. 532-537.

[37] Fertig, M. and Fruehauf. H., "Detailed Computation of the Aerothermodynamic Loads of the MIRKA Capsule," *3rd European Symposium on Aerothermodynamics*, Nov. 1998, pp. 703-710.

[38] Fruehauf, H., Fertig, M., and Kanne, S., "Validation of the Enhanced URANUS Nonequilibrium Navier-Stokes Code," *Journal of Spacecraft and Rockets*, Vol. 37, No. 2, 2000, pp. 218-223.

[39] Macret, J. and Leveugle, T., " The ARD Program: An Overview," AIAA Paper No. 99-4934, Jun. 1999.

[40] Tran, P. and Soler, J., "Atmospheric Reentry Demonstrator Post Flight Analysis: Aerothermal Environment," *Proceedings of the 2nd International Symposium on Atmospheric Reentry Vehicles*, Arcachon, France, Mar. 2001.

[41] Thirkettle, A., Steinkopf, M., and Joseph-Gabriel, E., "The Mission and Post-Flight Analysis of the Atmospheric Reentry Demonstrator," ESA Bulletin 109, Feb. 2002, pp. 56-63.

[42] Brown, J.L., "Turbulence Model Validation for Hypersonic Flows," AIAA Paper 2002-3308.

[43] Baldwin, B. and Lomax, H., "Thin Layer Approximation and Algebraic Model for Separated Turbulent Flows," AIAA Paper 78-257, Jan. 1978.

[44] Spalart, P. and Allmaras, S., "A One-Equation Turbulence Model for Aerodynamic Flows," AIAA Paper 92-0439, Jan. 1992.

[45] Wilcox, D., *Turbulence Modeling for CFD*, DCW Industries Inc., La Cañada, CA, 2nd Ed., 1998.

[46] Menter, F., "Two-Equation Eddy-Viscosity Turbulence Models for Engineering Applications," *AIAA Journal*, Vol. 32, No. 8, 1994, pp. 1598-1605.

[47] Hollis, B. and Perkins, J., "Comparisons of Experimental and Computational Aerothermodynamics of a 70° Sphere-Cone," AIAA Paper 96-1867, Jun. 1996.

[48] Shur, M., Spalart, P., Strelets, M., and Travin, A., "Detached Eddy Simulation of an Airfoil at High Angle of Attack," *4th International Symposium on Engineering Turbulence Modeling, Corsica*, 1999.

[49] Forsythe, J., Hoffman, K., and Squires, K., "Detached-Eddy Simulation with Compressibility Corrections Applied to a Supersonic Axisymmetric Base Flow," AIAA Paper 2002-0586, Jan. 2002.